Numerical simulations of stellar winds: polytropic models

R. Keppens and J.P. Goedbloed

FOM-Institute for Plasma-Physics Rijnhuizen, P.O. Box 1207, 3430 BE Nieuwegein, The Netherlands (e-mail: keppens@rijnh.nl; jpg@rijnh.nl)

Abstract. We discuss steady-state transonic outflows obtained by direct numerical solution of the hydrodynamic and magneto-hydrodynamic equations. We make use of the Versatile Advection Code, a software package for solving systems of (hyperbolic) partial differential equations. We proceed stepwise from a spherically symmetric, isothermal, unmagnetized, non-rotating Parker wind to arrive at axisymmetric, polytropic, magnetized, rotating models. These represent 2D generalisations of the analytical 1D Weber-Davis wind solution, which we obtain in the process. Axisymmetric wind solutions containing both a 'wind' and a 'dead' zone are presented.

Since we are solving for steady-state solutions, we efficiently exploit fully implicit time stepping. The method allows us to model thermally and/or magneto-centrifugally driven stellar outflows. We particularly emphasize the boundary conditions imposed at the stellar surface. For these axisymmetric, steady-state solutions, we can use the knowledge of the flux functions to verify the physical correctness of the numerical solutions.

Key words: Sun: solar wind – methods: numerical – Magnetohydrodynamics (MHD)

1. Introduction

Observational and theoretical research on stellar winds and astrophysical jets has evolved rapidly. For our own sun and its associated solar wind, the current understanding necessitates the combined study of solar wind acceleration and coronal heating in time-dependent modeling (Holzer & Leer 1997). At the same time, Holzer and Leer rightfully stressed that it remains useful to emphasize on early studies of wind acceleration. This, we find, is especially true for numerical modeling of stellar winds. With the ultimate goal of time-dependent heating/wind modeling in mind, we here address the simpler question on how to accurately model 1D and 2D steady-state winds by the numerical solution of the polytropic magnetohydrodynamic (MHD) equations.

Since much of the 1D solutions we obtain is known from the outset, we can verify our results *precisely*. Indeed, 1D Parker

(1958) and Weber-Davis (Weber & Davis 1967) wind solutions can be checked to agree with the analytic description. In their axisymmetric 2D extensions, various physical quantities must be conserved along poloidal streamlines. Sakurai (1985, 1990) presented such 2D generalizations of the magnetized Weber-Davis wind, using a method designed from these conservation laws. With modern numerical schemes, we can recover and extend his solutions to allow for the self-consistent modeling of 'dead' and 'wind' zones, as in the solar wind. Our steady-state solutions can be checked to conserve quantities along streamlines *a posteriori*.

Of crucial importance is the choice of boundary conditions used in the simulations. Since the governing equations for steady-state, transonic MHD flows are of mixed-type, their character can change from elliptic to hyperbolic at a priori undetermined internal critical surfaces. Causality arguments have been used to discuss which and how many boundary conditions must be prescribed (Bogovalov 1997). Our choice of boundary conditions used at the stellar surface is therefore discussed in detail.

All solutions presented are obtained with a single software package, the Versatile Advection Code (VAC, see Tóth 1996, 1997 and also `http://www.phys.uu.nl/~toth`). Although we only present steady-state transonic outflows in spherical and axisymmetry, VAC is developed for handling hydrodynamic (HD) and magnetohydrodynamic (MHD) one-, two-, or three-dimensional, steady-state or time-dependent problems in astrophysics. It is therefore capable of achieving our ultimate goal of time-dependent 3D wind modeling. The insight gained in this study of steady-state polytropic flows will then be very useful.

In Sect. 2, we list the equations and discuss the Versatile Advection Code for solving them in Sect. 3. Our calculations are presented in Sects. 4, 5, and 6. Conclusions are given in Sect. 7. The approach taken is a gradual one, where for instance our 1D solutions are used to construct initial conditions for their 2D extension. We will therefore model, in increasing order of complexity: (i) isothermal, spherically symmetric Parker winds; (ii) polytropic, spherically symmetric Parker winds; (iii) polytropic, rotating Parker winds for the equatorial plane; (iv) Weber-Davis magnetized, polytropic, rotating winds for the equatorial plane; and finally axisymmetric, poly-

tropic, rotating 2D winds, both (v) unmagnetized and magnetized, without (vi) and with (vii) a 'dead' zone.

2. Equations

We solve the HD and MHD equations expressed in the conservative variables density ρ, momentum vector $\rho\mathbf{v}$, and magnetic field $\mathbf{B}$. These are given by

$$\frac{\partial \rho}{\partial t} + \nabla \cdot (\rho\mathbf{v}) = 0, \tag{1}$$

$$\frac{\partial (\rho\mathbf{v})}{\partial t} + \nabla \cdot [\rho\mathbf{v}\mathbf{v} + p_{tot}\mathbf{I} - \mathbf{B}\mathbf{B}] = \rho\mathbf{g}, \tag{2}$$

$$\frac{\partial \mathbf{B}}{\partial t} + \nabla \cdot (\mathbf{v}\mathbf{B} - \mathbf{B}\mathbf{v}) = 0. \tag{3}$$

We introduced $p_{tot} = p + \frac{1}{2}B^2$ as the total pressure, $\mathbf{I}$ as the identity tensor, $\mathbf{g}$ as the external gravitational field, and exploited magnetic units such that the magnetic permeability is unity. We drop the energy equation and assume a polytropic relation connecting the thermal pressure p and the density ρ. For a polytropic index γ, we thus assume $p \sim \rho^\gamma$. Hence, we do not address the heat deposition in the corona. Although we solve the time-dependent equations as given above, we will only present steady-state $\partial/\partial t = 0$ solutions of Eqs. (1)–(3). For stellar wind calculations, we consider a spherically symmetric external gravitational field $\mathbf{g} = -GM_*/r^2 \hat{\mathbf{e}}_r$, where G is the gravitational constant, M_* is the stellar mass, r is the distance to the stellar center, and $\hat{\mathbf{e}}_r$ indicates the radial unit vector.

3. Versatile advection code

In this section, we discuss the software and numerical method used. The physics results are described from Sect. 4 onwards. The Versatile Advection Code (VAC, see Tóth 1996, 1997) is a general purpose software package for solving a conservative system of hyperbolic partial differential equations with additional non-hyperbolic source terms, such as the MHD equations. VAC runs on PC's, on a variety of workstations, on vector platforms, and we can also run in parallel on a cluster of workstations, and on distributed memory architectures like the Cray T3D and T3E, and the IBM SP (Keppens & Tóth 1998, Tóth & Keppens 1998). The code is written in the dimension independent LASY syntax (Tóth 1997), so it can be used as a convenient tool to handle HD and MHD one-, two-, or three-dimensional problems in astrophysics and laboratory plasma physics. The dimensionality of the problem and the actual set of equations to solve are easily selected in a preprocessing step.

VAC uses a structured finite volume grid and offers a choice of conservative, second order accurate, shock-capturing, spatial and temporal discretization schemes. The spatial discretizations include two Flux Corrected Transport variants and four Total Variation Diminishing (TVD) schemes (Tóth & Odstrčil 1996). Temporal discretization can be explicit, semi-implicit, or fully implicit. It was recently demonstrated (Keppens et al. 1998, Tóth et al. 1998) how the implicit approach can be used very

efficiently, for steady-state and time-accurate problems possibly containing discontinuities. Here, we expect smooth solutions to the steady-state HD and MHD equations, so one can greatly benefit computationally from fully implicit time stepping.

In this paper, we solve the polytropic HD ($\mathbf{B} = 0$) Eqs. (1) and (2) in Sects. 4.1 and 5. Magnetohydrodynamic equations are solved in Sects. 4.2 and 6. We solve one-dimensional problems in Sect. 4 and two-dimensional problems in Sects. 5 and 6. In practice, this means that the stellar winds we model are solutions of the equations under the additional assumption of a prescribed symmetry in the ignored directions. One-dimensional problems assume a spherical symmetry, while 2D solutions assume $\partial/\partial\varphi = 0$. Here, φ denotes the angle in a cylindrical (R, φ, z) coordinate system centered on the star with its polar and rotation axis as z-axis.

Since we are interested in steady-state solutions, we use fully implicit time stepping as detailed and demonstrated in Keppens et al. (1998) and Tóth et al. (1998). The linear systems arising in the linearized fully implicit backward Euler scheme are solved using a direct block tridiagonal solver for the 1D problems and using a preconditioned Stabilized Bi-Conjugate Gradient iterative solver (van der Vorst 1992) for the 2D cases. The Modified Block Incomplete LU preconditioner is described in van der Ploeg et al. (1997). We consistently used the TVD Lax-Friedrich (TVDLF) spatial discretization (Yee 1989, Tóth & Odstrčil 1996) using *Woodward* limiting (Collela & Woodward 1984). We typically took Courant numbers $C = \mathcal{O}(100)$. For all 1D solutions and for the 2D hydrodynamic solutions, the steady-state is reached when the relative change in the conservative variables from one time level to the next drops below 10^{-8}. We use a normalized measure defined by (Tóth et al. 1998)

$$\Delta_2 U \equiv \sqrt{\frac{1}{N_{\text{var}}} \sum_{u=1}^{N_{\text{var}}} \frac{\sum_{\text{grid}}(U_u^{n+1} - U_u^n)^2}{\sum_{\text{grid}}(U_u^n)^2}}, \tag{4}$$

where N_{var} is the number of conserved variables U_i, and the superscripts indicate the pseudo time level t^n. Since we are solving for smooth solutions, the numerical schemes can easily achieve such accuracy in the steady-state solutions.

For the axisymmetric 2D MHD solutions, the way to ensure a zero divergence of the magnetic field is non-trivial. Unless one uses a scheme which keeps $\nabla \cdot \mathbf{B} = 0$ exactly in some discretization, like the constrained transport method (Evans & Hawley 1988), corrective action needs to be taken during the time integration. This involves either including corrective source terms in the equations which are proportionate to the numerically generated divergence (Powell 1994, their use for TVDLF was first advocated by Tóth & Odstrčil 1996), or making use of a projection scheme (Brackbill & Barnes 1980) which involves the solution of a Poisson equation. These two approaches can even be combined and such combination is also beneficial for fully implicit schemes (Tóth et al. 1998). For the 2D axisymmetric MHD wind solutions presented in Sect. 6, it proved difficult to ensure a divergence free solution in a fully implicit manner. Using explicit time stepping and employing the projection scheme before every time step, we could get steady-state solutions where

$\Delta_2 U \simeq \mathcal{O}(10^{-7})$ which have acceptable $\mid \nabla \cdot \mathbf{B} \mid < 10^{-3}$, although this time-marching method is computationally much more costly than the implicit approach. The use of Powell source terms alone proved inadequate for these wind solutions, as fairly large errors are then advected into the whole solution domain from the stellar boundary outwards.

VAC makes use of two layers of ghost cells surrounding the physical domain to implement boundary conditions. A symmetry condition at a boundary is then imposed by mirroring the calculated values in the two physical cell layers adjacent to the boundary in these ghost cells. The boundary conditions imposed at the stellar surface are extremely important. We will emphasize them for all cases considered.

4. 1D polytropic winds

4.1. Parker winds

Our starting point is the well-known analytic Parker (1958) solution for a spherically symmetric, isothermal ($\gamma = 1$) outflow from a star of mass M_* and radius r_*. Given the magnitude of the escape speed $v_{esc} = \sqrt{2GM_*/r_*}$, one can construct a unique 'wind' solution which starts subsonically at the stellar surface and accelerates monotonically to supersonic speeds. This solution is transonic at the critical position $r_s = v_{esc}^2 r_*/(4c_{s*}^2)$, where $c_{s*}^2 = p/\rho$ is the constant isothermal sound speed. Since we know the position of the critical point r_s, we can easily determine the flow profile $v_r(r)$ and the corresponding density profile $\rho(r)$. The radial velocity is obtained from the iterative solution of the transcendental equation

$$\frac{v_r}{c_{s*}} = \sqrt{4\left(\frac{r_s}{r}\right) - 3 + 2\ln\left[\left(\frac{r}{r_s}\right)^2 \left(\frac{v_r}{c_{s*}}\right)\right]}. \tag{5}$$

The density profile results from the integrated mass conservation equation. Since the radial velocity reaches a constant supersonic value asymptotically, the corresponding density vanishes at infinity as $1/r^2$.

Choosing units such that $r_* = 1$, $\rho_* \equiv \rho(r_*) = 1$ with $c_{s*} = 1$, we initialize a 1D spherically symmetric, polytropic (with $\gamma > 1$) hydrodynamic outflow with this analytic isothermal Parker wind solution on a non-uniform mesh ranging through $r \in [1, 50]r_*$. We use 1000 grid points and exploit a grid accumulation at the stellar surface, where the acceleration due to the pressure gradient is largest. In the ghost cells used to impose boundary conditions at the stellar surface, we fix the value of the base density to unity, and extrapolate the radial momentum continuously from its calculated value in the first grid cell. At $r = 50r_*$, we extrapolate both density and radial momentum continuously into the ghost cells. We then use a fully implicit time integration to arrive at the corresponding steady-state, spherically symmetric, polytropic Parker wind solution. The obtained solution $\rho(r)$, $v_r(r)$ can be verified to have a constant mass flux $\rho r^2 v_r$ as a function of radius and energy integral

$$E = \left(v_r^2/2 + c_s^2/(\gamma - 1) - GM_*/r\right)/c_{s*}^2,$$

where $c_s^2(r) = \rho^{\gamma-1}$. Also, determining the sonic point r_s where $v_r(r_s) = c_s(r_s)$ and the base radial velocity v_{r*}, the solution can be checked to satisfy

$$\frac{r_s}{r_*} = \left(\frac{v_{esc}}{2c_{s*}}\right)^{\frac{2(\gamma+1)}{5-3\gamma}} \left(\frac{c_{s*}}{v_{r*}}\right)^{\frac{2(\gamma-1)}{5-3\gamma}}. \tag{6}$$

Note how the isothermal $\gamma = 1$ case is the only polytropic wind solution where the position of the critical point can be determined *a priori*.

In practice, we increased the polytropic index gradually from $\gamma = 1$ through 1.05, 1.1, 1.12, 1.125 to $\gamma = 1.13$, each time relaxing the obtained steady-state solution for one polytropic index to the unique transonic wind solution for the next value. In the top panel of Fig. 1, we plot the radial variation of the Mach number $M_s = v_r/c_s$ for the isothermal $\gamma = 1$ Parker wind with $v_{esc} = 3.3015c_{s*}$, and for similar polytropic winds with $\gamma = 1.1$ and 1.13. The vertical dashed lines indicate the agreement of the positions of the sonic points where $M_s = 1$ with the calculated right hand side of Eq. (6). Note the outward shift of the sonic point with increasing polytropic index and the corresponding decrease of the asymptotic radial velocity.

When we relax the restriction of spherical symmetry by allowing a rigid stellar rotation rate Ω_*, we can easily construct a solution for the equatorial plane only. Indeed, ignoring variations perpendicular to this plane, one simply adds a toroidal velocity profile where $v_\varphi(r) = \Omega_* r_*(r_*/r)$ and then solves for $\rho(r)$, $v_r(r)$, and $v_\varphi(r)$. The boundary conditions on the toroidal momentum keep ρv_φ fixed at the base and extrapolate it continuously at the end of the computational domain. A polytropic, rotating Parker solution for the equatorial regions is found by relaxation from a non-rotating wind with the same polytropic index γ. In the bottom panel of Fig. 1, we show the Mach number $M_s(r)$ for $v_{esc} = 3.3015c_{s*}$ and $\gamma = 1.13$ Parker winds where $\zeta = \Omega_* r_*/c_{s*}$ equals $\zeta = 0.0156$, $\zeta = 1$ and $\zeta = 1.9$. The solution with $\zeta = 0.0156$ hardly differs from its non-rotating thermally driven counterpart shown in Fig. 1, as expected. The additional centrifugal acceleration causes an increase in the base velocity v_{r*} and in the asymptotic radial velocity. Again, the solution can be verified to have a constant radial mass flux $\rho r^2 v_r$, Bernoulli function

$$E = \left([v_r^2 + v_\varphi^2]/2 + c_s^2/(\gamma - 1) - GM_*/r\right)/c_{s*}^2,$$

and constant specific angular momentum $r v_\varphi$. The positions of the critical point(s) r_s are now obtained from a generalization of Eq. (6), namely from the solutions of

$$\zeta^2 \left(\frac{r_*}{r_s}\right)^2 - \frac{v_{esc}^2 r_*}{2c_{s*}^2 r_s} + 2\left[\left(\frac{v_{r*}}{c_{s*}}\right)\left(\frac{r_*}{r_s}\right)^2\right]^{\frac{2(\gamma-1)}{\gamma+1}} = 0. \tag{7}$$

This equation reduces to a second degree polynomial for a $\gamma = 1$ isothermal, rotating, Parker wind so it is evident that rotation rates exist that introduce a second critical point. In Fig. 1, only the $\zeta = 1.9$ solution exhibits two critical points, shown as vertical dotted lines, within the domain. We determined the critical
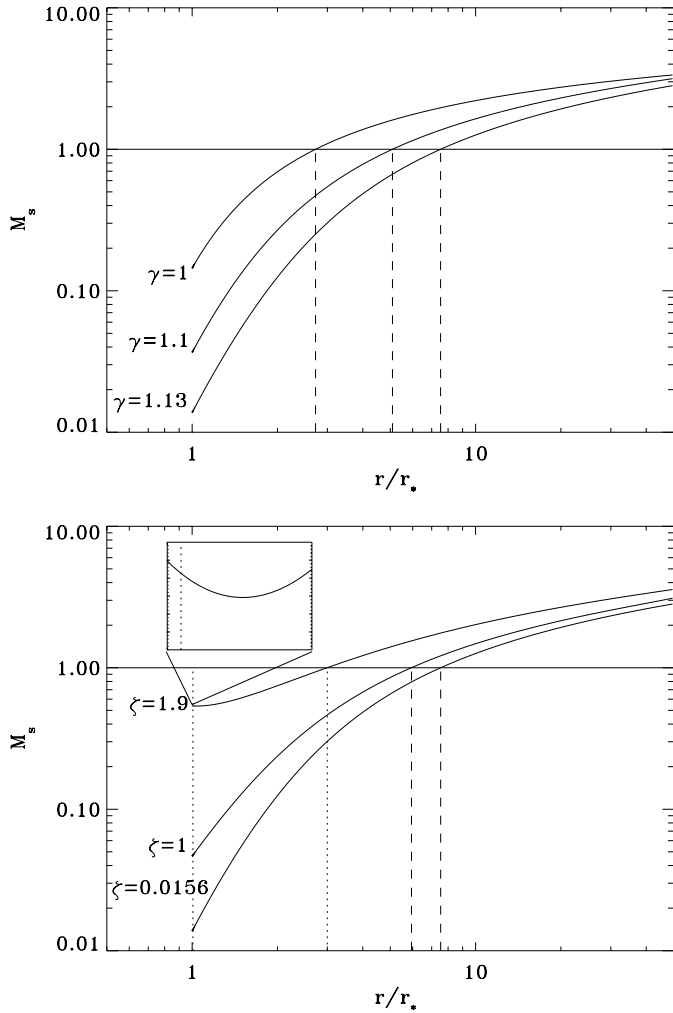
Fig. 1. Polytropic Parker winds with $v_{esc} = 3.3015c_{s*}$. *Top panel:* Mach number M_s as a function of radial coordinate for spherically symmetric Parker winds for polytropic index $\gamma = 1$ (isothermal), $\gamma = 1.1$ and $\gamma = 1.13$. *Bottom panel:* equatorial solutions for rotating $\gamma = 1.13$ polytropic Parker winds for various rotation parameters ζ. Critical points are indicated.

point(s) by solving Eq. (7) using the calculated base speed v_{r*}. The close-up of the radial variation of M_s for $\zeta = 1.9$ at the base reveals that this thermo-centrifugally driven wind passes the first critical point while being decelerated, then starts to accelerate and finally becomes supersonic at the second critical point. To correctly capture the dynamics close to the stellar surface it is clear that we need a high grid resolution, especially at the stellar surface. Indeed, the first critical point for the $\zeta = 1.9$ solution is situated at $1.006r_*$.

4.2. Weber-Davis winds

The magnetized Weber-Davis (WD) solution (Weber & Davis 1967) represents a valuable extension to the rotating, polytropic Parker wind solution for the equatorial plane. Again assuming that there is no variation perpendicular to this plane, one now needs to solve for an additional two magnetic field components

$B_r(r)$ and $B_\varphi(r)$. One is trivially obtained from the $\nabla \cdot \mathbf{B} = 0$ equation, namely $B_r = B_{r*}r_*^2/r^2$. The analytic treatment reveals that the magnetized polytropic wind solution has a total of two critical points, namely the slow r_s and the fast r_f critical point. These are determined by the zeros of $v_r^4 - v_r^2(c_s^2 + A_r^2 + A_\varphi^2) + c_s^2 A_r^2$. In between lies the Alfvén point r_A, defined as the radius at which the radial velocity v_r equals the radial Alfvén speed $A_r = B_r/\sqrt{\rho}$. Since the equatorial fieldline is prescribed to be radial in the poloidal plane and the transfield force balance is not taken into account, this Alfvénic transition is not a critical point in this model.

In the fully implicit time stepping towards a steady-state WD wind for specific values of $v_{esc} = 3.3015c_{s*}$, $\gamma = 1.13$, $\zeta = 0.0156$, and for the base radial Alfvén speed $A_{r*} = B_{r*}/\sqrt{\rho_*} = 3.69c_{s*}$, we initialize $\rho(r)$, $v_r(r)$, and $v_\varphi(r)$ with the corresponding non-magnetic, polytropic rotating Parker solution. We fix B_r to its known $1/r^2$ dependence throughout the time evolution, and initialize B_φ to zero. The boundary conditions at $r = 50r_*$ extrapolate all quantities we solve for continuously into the ghost cells. At the base, we keep the density fixed, the radial momentum and toroidal field component are extrapolated linearly from the first two calculated mesh points, while the toroidal momentum ρv_φ is coupled to the magnetic field ensuring

$$\frac{v_\varphi - \Omega_* r_*}{v_r} = \frac{B_\varphi}{B_r}. \tag{8}$$

This expresses the parallelism of the velocity and the magnetic field in the frame rotating with the stellar angular velocity Ω_*. Using these initial and boundary conditions, we arrive at the unique WD wind solution for the given parameters. This magnetized polytropic wind solution for the equatorial plane is shown in Fig. 2. The solution agrees *exactly* with the analytic WD wind: we obtain five constants of motion, namely the mass flux $\rho r^2 v_r \simeq 0.0139$, the magnetic flux $r^2 B_r = 3.69$ which is constant by construction, the validity of Eq. (8) over the whole domain, the Bernoulli integral

$$E = \left([v_r^2 + v_\varphi^2]/2 + c_s^2/(\gamma - 1) - GM_*/r - v_\varphi B_\varphi B_r/\rho v_r \right.$$
$$\left. + B_\varphi^2/\rho\right)/c_{s*}^2 \simeq 2.45,$$

and the constant total specific angular momentum $L = rv_\varphi - rB_\varphi B_r/\rho v_r \simeq 13.36$. The positions of the critical points are $r_s = 7.4r_*$ and $r_f = 31.2r_*$, while the Alfvén point is at $r_A = 29.2r_*$, as indicated in Fig. 2. This agrees with the values given in the Appendix to Keppens et al. (1995), where the same WD solution was calculated in a completely different fashion. Indeed, the WD solution for given values of γ, c_{s*}, v_{esc}/c_{s*}, ζ, and A_{r*}/c_{s*}, can alternatively be calculated as a minimization problem in a six-dimensional space (see Belcher & MacGregor 1976) where one solves for the six unknowns $[v_{r*}, v_{\varphi*}, r_s, v_r(r_s), r_f, v_r(r_f)]$. This can be done using standard Newton-Raphson iteration provided one has an educated initial guess, but it can even be obtained by the use of a *genetic algorithm*, as first demonstrated by Charbonneau (1995). The fact that the, for our method initially unknown, base velocities appear in the determining set of variables for these minimization methods again indicates that a high base resolution
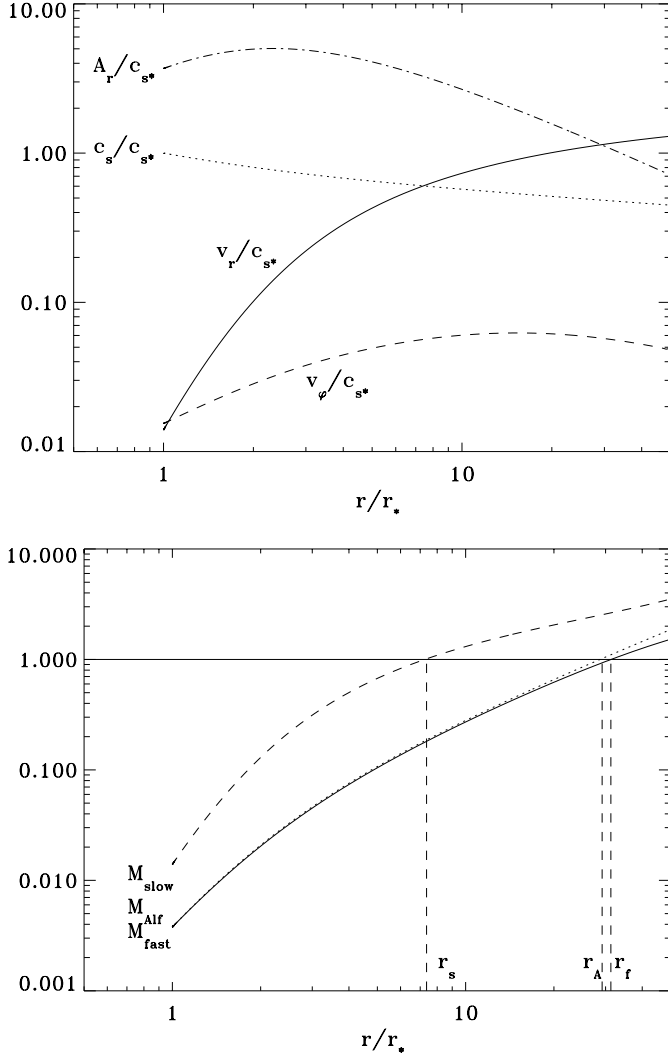
Fig. 2. Weber-Davis wind solution for the equatorial plane. *Top panel:* radial variation of the radial Alfvén speed A_r, sound speed c_s, and velocities v_r and v_φ, all normalized to the base sound speed c_{s*}. *Bottom panel:* the corresponding poloidal Alfvén Mach number $M_A = v_r/A_r$, and poloidal slow and fast Mach numbers, determining the positions of the critical points and the Alfvén point. See text for parameters.

is absolutely essential. Values for these six unknowns found from the solution in Fig. 2 are $[0.01395, 0.01541, 7.4, 0.6018, 31.2, 1.1592]$ and these agree with the Newton-Raphson solution.

The calculation of the WD polytropic wind by the stepwise relaxation from an isothermal Parker wind is thus an excellent test for the numerics, as every step (from isothermal to polytropic, from non-rotating to rotating, from Parker to WD) can be verified *precisely* to agree with the known solutions. It should be clear that we can construct WD wind solutions where the acceleration results from the combined action of thermal, centrifugal, and magnetic forces. However, our interest is in the generalization of these 1D models out of the equatorial plane. We will again proceed in logical steps towards this goal.

5. Axisymmetric 2D polytropic HD winds

To arrive at a crude model for the coronal expansion of a rigidly rotating star, we set forth to construct an axisymmetric, steady-state, polytropic wind solution valid throughout a poloidal cross-section. With the polar axis as rotation and symmetry axis, we need to generalize the rotating, polytropic Parker wind which succesfully modeled the equatorial regions. Whereas the Parker solution had at least one critical point, its 2D extension is expected to give rise to critical curves in the poloidal plane. The degree of rotation determines the deviation from perfect circles arising in the non-rotating, spherically symmetric case.

To initialize a 2D fully implicit time-stepping procedure to arrive at a steady-state wind, we use the 1D Parker solution with identical escape speed v_{esc}, polytropic index γ, and rotational parameter ζ. We use a spherical (r, θ) grid in the poloidal plane, where the grid spacing is equidistant in θ, but is accumulated at the base in the radial direction. We take a 300×20 grid and only model a quarter of a full poloidal cross-section. The density is initialized such that for all angles θ, the radial variation equals the 1D Parker wind appropriate for the equator. Writing the Parker solution as $\rho^P(r)$, $v_r^P(r)$, $v_\varphi^P(r)$, we set $\rho(r, \theta; t = 0) = \rho^P(r)$, and similarly, we set $v_r(r, \theta; t = 0) = v_r^P(r)$ and $v_\varphi(r, \theta; t = 0) = v_\varphi^P(r)\sin(\theta)$ so that it vanishes at the pole $\theta = 0$, while $v_\theta(t = 0) = 0$ everywhere. Since we now use a coarser radial resolution, we interpolate the Parker solution linearly onto the new radial grid. Boundary conditions then impose symmetry conditions at the pole ($\theta = 0$) and the equator ($\theta = \pi/2$). The radial coordinate still covers $r \in [1, 50]r_*$, as in the 1D calculations. Since the solutions are supersonic at $r = 50r_*$, the boundary conditions there merely extrapolate the density and all three momentum components linearly in the ghost cells. The stellar rotation enters as a boundary condition in the toroidal momentum component, which enforces $v_\varphi = \Omega_* R_*$, where (R, z) are the cartesian coordinates in the poloidal (r, θ) plane. Note that the toroidal momentum may still change in the process, since we can no longer fix the density at the stellar surface to a θ-independent constant value. This is because in steady-state, the density profile should establish a gradient in the θ direction to balance the component of the centrifugal force in that direction. In the purely radial direction, the inwards pointing gravity must be balanced by the combination of the pressure gradient and the radial component of the centrifugal force. We therefore extrapolate the density linearly at the base. To enforce the total mass flux as in the equatorial Parker solution, we determine the constant $f_{mass} = \rho^P r^2 v_r^P$ from the 1D calculation, and fix $\rho v_R = f_{mass}R/r^3$ and $\rho v_z = f_{mass}z/r^3$ at the stellar surface for its 2D extension.

An elementary analytic treatment for a 2D polytropic steady-state wind solution proceeds by noting that mass conservation is ensured when the poloidal momentum is derived from an arbitrary stream function $\chi(R, z)$ such that $\rho \mathbf{v}_p = (1/R)\hat{e}_\varphi \times \nabla\chi$. It is then easily shown that the toroidal momentum equation is equivalent with the existence of a second arbitrary function $L(\chi) = Rv_\varphi$, corresponding to the conserva-

tion of specific angular momentum along a poloidal streamline. Similarly, energy conservation along a streamline introduces

$$E(\chi) = \left[v_R^2 + v_z^2 + v_\varphi^2\right]/2 + \rho^{\gamma-1}/(\gamma-1) - GM_*/r.$$

Across the poloidal streamlines all forces must balance out.

We show streamlines and the contours of constant poloidal Mach number $M_p = \sqrt{(v_R^2 + v_z^2)/c_s^2}$ for two hydrodynamic wind solutions for $v_{esc} = 3.3015c_{s*}$, $\gamma = 1.13$, and with $\zeta = 0.0156$ (top panel) and $\zeta = 0.3$ (bottom panel) in Fig. 3. We restricted the plotting region to about $10r_*$. For the imposed mass flux parameter, we used the values $f_{mass} = 0.01377$ for the slow rotator and $f_{mass} = 0.01553$ for the faster rotator, as found from the equatorial Parker solution for the same γ and ζ. Note how for low rotation rates, the wind solution is almost spherically symmetric with nearly radial streamlines and circular Mach curves. For higher rotation rates, the critical Mach curve where $M_p = 1$ moves inwards at the equator and outwards at the pole when compared to a non-rotating case. The streamlines show the equatorward deflection when material is released from the stellar surface due to the centrifugal force. Such equatorward streamline bending due to rotation is discussed in detail in the analytical study by Tsinganos & Sauty (1992). For these solutions, we can then verify that the specific angular momentum L, as well as the total energy E, are conserved along the streamlines.

6. Axisymmetric 2D polytropic MHD winds

6.1. Magnetized winds

To obtain an axisymmetric magnetized wind solution, we may simply add a purely radial magnetic field to a 2D HD wind solution and use this configuration as an initial condition for an MHD calculation. Hence, we set $B_R(R, z; t = 0) = \beta R/r^3$ and $B_z(R, z; t = 0) = \beta z/r^3$ while $B_\varphi(t = 0) = 0$. Such a monopolar field is rather unrealistic for a real star, but it is the most straightforward way to include magnetic effects. The same type of field was used by Sakurai (1985, 1990), which contained the first 2D generalization of the WD model.

Boundary conditions at equator and pole are imposed by symmetry considerations. At $r = 50r_*$, we extrapolate all quantities linearly. Similarly, the base conditions extrapolate the density profile ρ and all magnetic field components, while the poloidal velocity components are set to ensure a prescribed mass flux. The stellar rotation rate and the coupling between the velocity and the magnetic field enters in the boundary condition at the stellar surface where we demand

$$v_\varphi = \Omega_* R_* + B_\varphi\sqrt{v_R^2 + v_z^2}/\sqrt{B_R^2 + B_z^2}. \tag{9}$$

Specific attention is paid to ensuring the $\nabla \cdot \mathbf{B} = 0$ condition. As explained in Sect. 3, we now switch strategy and use explicit time stepping combined with a projection scheme to obtain the steady state solution.

We calculated the 2D extension of the WD wind corresponding to $v_{esc} = 3.3015c_{s*}$, $\gamma = 1.13$, $\zeta = 0.0156$ and $\beta = 3.69$. The mass flux is set to be $f_{mass} = 0.01377$. We show in Fig. 4
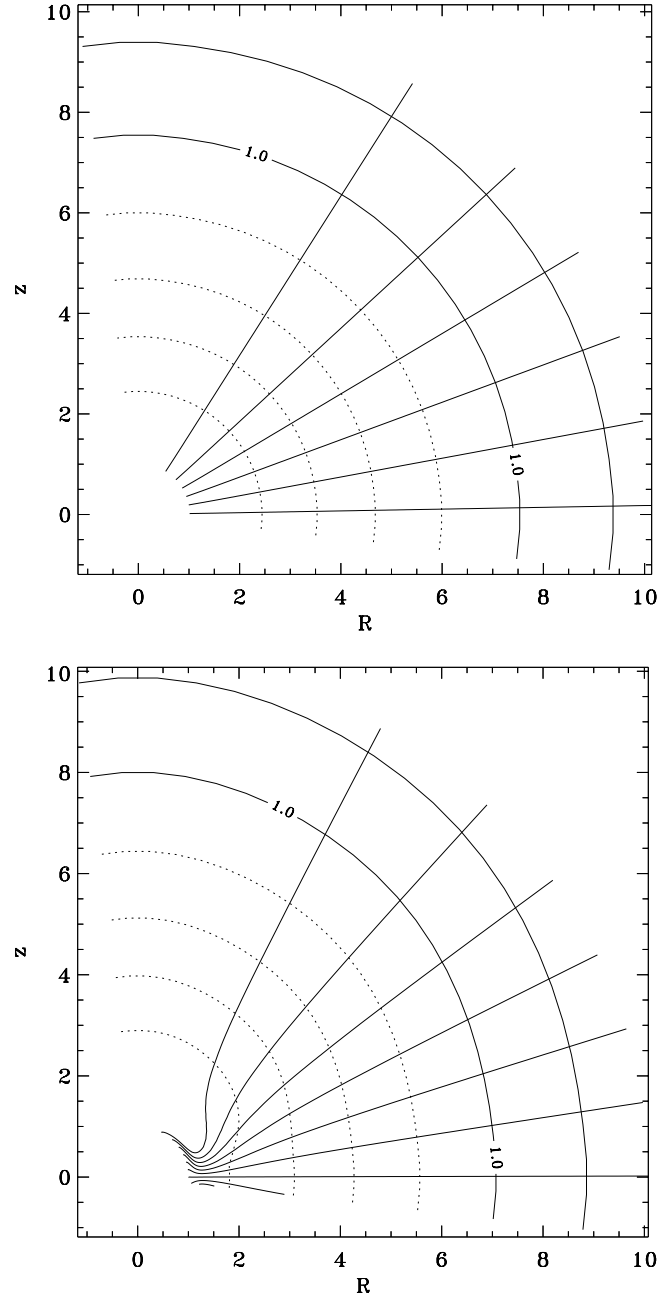

Fig. 3. 2D Polytropic HD winds. We show streamlines and contours (dotted for values below unity) of the poloidal Mach number M_p in the poloidal plane. For low (*top panel*) and high (*bottom panel*) rotation rates.

the streamlines, and the positions of the critical curves where the poloidal Alfvén Mach number and the poloidal slow and fast Mach numbers equal unity. The squared poloidal Alfvén Mach number M_A^p is given by

$$\left(M_A^p\right)^2 = \left(v_R^2 + v_z^2\right)/\left(A_R^2 + A_z^2\right) \equiv \frac{v_p^2}{A_p^2}, \tag{10}$$

with Alfvén speeds $A_i \equiv B_i/\sqrt{\rho}$. The squared poloidal slow M_s^p and fast M_f^p Mach numbers are defined by
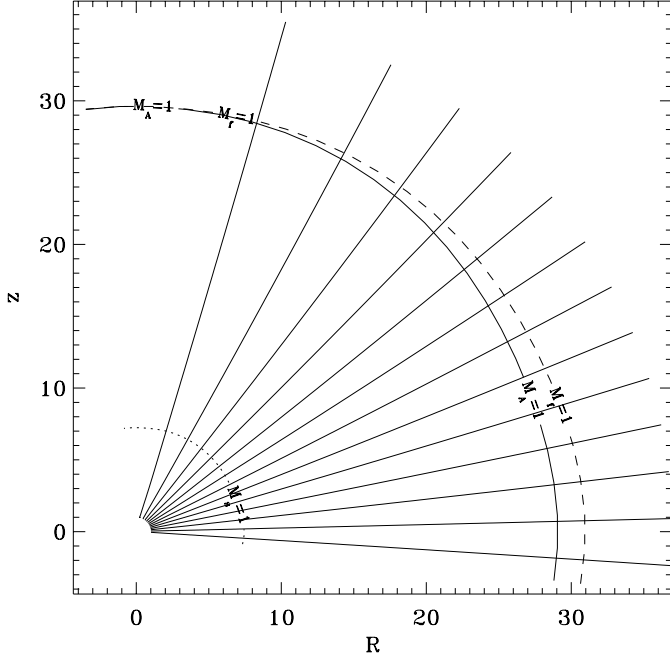
Fig. 4. Polytropic axisymmetric MHD wind. We show the streamlines and the positions of the critical surfaces where the poloidal Mach numbers equal unity. Parameters are as in the 1D Weber-Davis wind shown in Fig. 2.

$$(M_s^p)^2 = \frac{2\left(v_R^2 + v_z^2\right)}{c_s^2 + A_p^2 + A_\varphi^2 - \sqrt{\left[c_s^2 + A_p^2 + A_\varphi^2\right]^2 - 4\,c_s^2\,A_p^2}},$$
(11)

$$\left(M_f^p\right)^2 = \frac{2\left(v_R^2 + v_z^2\right)}{c_s^2 + A_p^2 + A_\varphi^2 + \sqrt{\left[c_s^2 + A_p^2 + A_\varphi^2\right]^2 - 4\,c_s^2\,A_p^2}}.$$
(12)

At the pole, the fast Mach number coincides with the Alfvén one since B_φ vanishes there and the parameters are such that $A_p^2 > c_s^2$. Away from the pole, the toroidal field component does not vanish, so that Alfvén and fast critical curves separate. Note how the equatorial solution strongly resembles the WD wind solution for the same parameters shown in Fig. 2. The obtained wind solution is mostly thermally driven, like the solar wind. The rotation rate and magnetic field effects are minor and an almost spherically symmetric wind results. Sakurai (1985, 1990) demonstrated that for stronger fields, the magnetic force of the spiraling fieldlines deflect the outflow poleward. This magnetic pinching force can produce a polar collimation of the wind. These effects have also been addressed by analytical studies of self-similar outflows in Trussoni et al. (1997).

For these axisymmetric, steady-state MHD outflows, the solutions can be verified to obey the following conservation laws. Mass conservation is ensured when writing the poloidal momentum vector as $\rho\mathbf{v}_p = (1/R)\hat{e}_\varphi \times \nabla\chi$, with the stream function $\chi(R,z)$. The zero divergence of the magnetic field yields, likewise, $\mathbf{B}_p = (1/R)\hat{e}_\varphi \times \nabla\psi$, with ψ the flux function. The poloidal part of the induction equation then leads to

$\chi(\psi)$, provided that the toroidal component of the electric field E_φ vanishes. This can easily be checked from $v_R B_z = v_z B_R$, and the solution shown in Fig. 4 satisfies this equality to within 1%. This allows us to write $\chi' \equiv d\chi/d\psi = \rho v_p/B_p = \rho v_R/B_R = \rho v_z/B_z$. A fair amount of algebra shows that the toroidal momentum and induction equation introduce two more flux functions, namely the specific angular momentum $L(\psi) = Rv_\varphi - RB_\varphi B_p/\rho v_p$ and a function related to the electric field $\Omega(\psi) = \left[v_\varphi - (v_p/B_p)B_\varphi\right]/R$. The Bernoulli function derivable from the momentum equation can be written as

$$\begin{aligned} E(\chi) =\ & \left[v_R^2 + v_z^2 + v_\varphi^2\right]/2 + \rho^{\gamma-1}/(\gamma-1) - GM_*/r \\ & - v_\varphi B_\varphi B_p/\rho v_p + B_\varphi^2/\rho. \end{aligned}$$

Note how the constants of motion found in the WD solution immediately generalize in this formalism (mass flux, magnetic flux, corotation as in Eq. (8), specific angular momentum L and Bernoulli function E). The hydrodynamic limit is found for zero magnetic field $\mathbf{B} = 0$ and vanishing electric field $\Omega = 0$. Across the poloidal streamlines, the momentum balance is governed by the generalized, mixed-type Grad-Shafranov equation. The numerical solutions we obtained indeed have parallel poloidal streamlines and poloidal fieldlines and conserve all these quantities along them.

6.2. Winds containing a 'dead' zone

The monopolar field configuration used above is unrealistic. However, it should be clear that our method easily generalizes to bipolar stellar fields by appropriately changing the initial condition on the magnetic field. In fact, a star like our sun has open fieldlines at both poles and closed fieldlines around its equator. To obtain a steady-state stellar wind containing a 'wind' zone along the open fieldlines and a 'dead' zone about the stellar equator, we can simply initialize the polar regions up to a desired polar angle θ_{wind} as above. The equatorial 'dead' zone is then initialized as follows: the density and the toroidal momentum component is taken from the 2D HD wind with the same rotational and polytropic parameters while the poloidal momentum components are set to zero. The initial magnetic field configuration in the 'dead' zone is set to a dipole field which has

$$B_R = 3a_d \frac{z\,R}{(R^2 + z^2)^{5/2}},$$
(13)

and

$$B_z = a_d \frac{(2z^2 - R^2)}{(R^2 + z^2)^{5/2}}.$$
(14)

The strength of the dipole is taken $a_d = \beta/(2\cos(\theta_{wind}))$ to keep the radial field component B_r constant at $\theta = \theta_{wind}$. The initial B_φ component is again zero throughout. In summary, we now have the following set of parameters used in the simulation: the escape speed v_{esc}, the polytropic index γ, the rotational parameter ζ, the field strength through β, and the extent of the dead zone through θ_{wind}. In addition, the mass flux f_{mass} is used in the boundary condition of the poloidal momentum components.
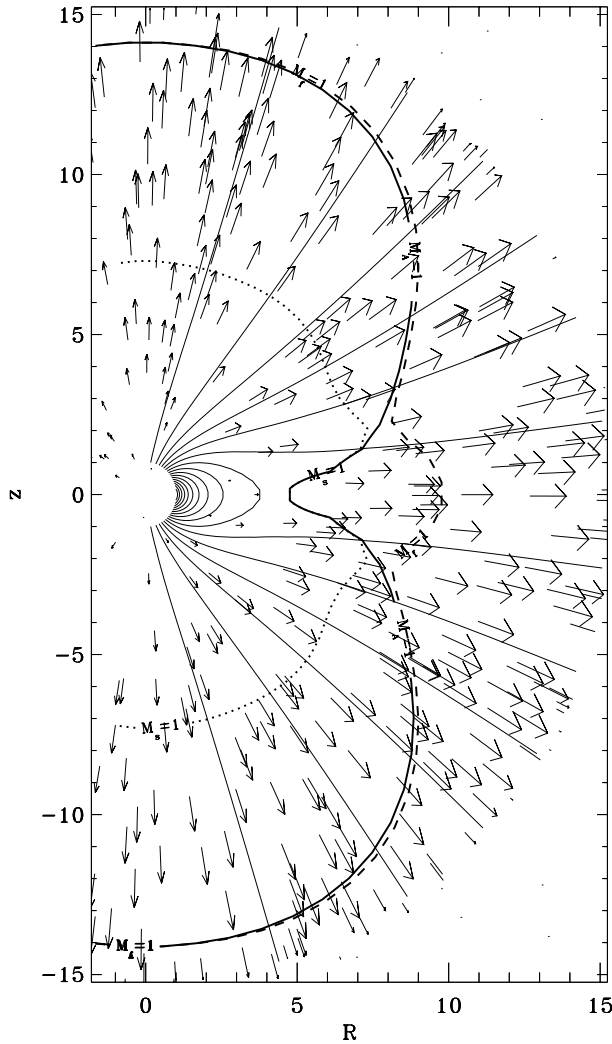
Fig. 5. Axisymmetric magnetized wind containing a 'wind' and a 'dead' zone. Shown are the poloidal magnetic fieldlines and the poloidal flow field as vectors. Indicated are the three critical surfaces where $M_s^p = 1$ (dotted), $M_A^p = 1$ (solid line), and $M_f^p = 1$ (dashed).

Fig. 6. Polar plots of the scaled density (dashed) and velocity (solid) for two fixed radial distances: 10 and 20 (thick lines) stellar radii. The 'dead' zone has a clear influence on the latitudinal variation.

Boundary conditions at the stellar surface are identical as above, but now the dead zone has a zero mass flux, so that $f_{mass}(\theta)$. Note that in a completely analoguous way, we could allow for a latitudinal dependence of the stellar rotation rate $\Omega_*(\theta)$, or the magnetic field strength $\beta(\theta)$.

This $t = 0$ guess for an axisymmetric MHD wind is then time-advanced to a stationary solution. Fig. 5 shows the final stationary state, for the parameter values $v_{esc} = 3.3015 c_{s*}$, $\gamma = 1.13$, a constant rotation rate corresponding to $\zeta = 0.0156$, $\beta = 3.69$, $\theta_{wind} = 60°$ and the mass flux in the wind zone set to the constant $f_{mass} = 0.01377$, while it is zero in the dead zone. These parameters are as in the WD solution and the Sakurai wind presented earlier. The initial field geometry has evolved to one where the open fieldlines are draped around a distinct bipolar 'dead' zone of limited radial extent and the prescribed latitudinal range. The outflow nicely traces the field geometry outside this dead zone. As seen from the figure, we have calcu-
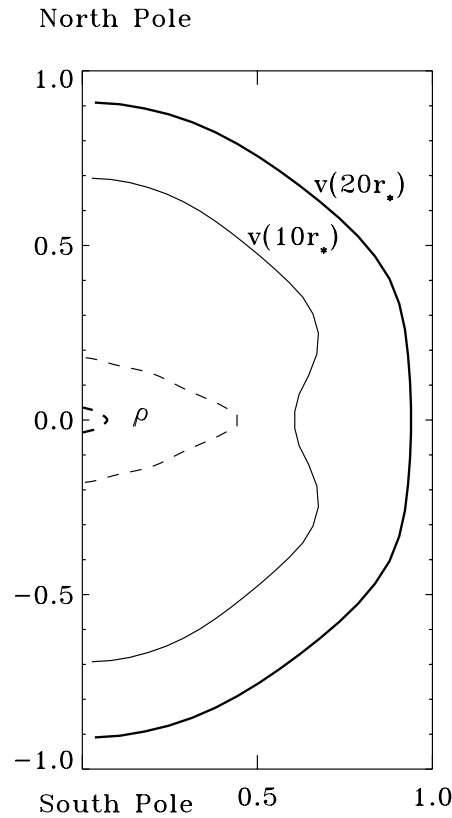
lated the full poloidal halfplane and imposed symmetry boundary conditions at north and south pole. We used a polar grid of resolution 300×40 of radial extent $[1, 50]r_*$ with a radial grid accumulation at the base. The north-south symmetry of the final solution is a firm check of the numerics. The critical surfaces are also indicated in Fig. 5 and they differ significantly from the monopolar field solution shown in Fig. 4. Again, at the polar regions, the Alfvén and fast critical surface coincides. Now, the B_φ also vanishes at the equator where conditions are such that the slow and the Alfvén critical surfaces coincide. The B_φ component changes sign when going from north to south, as the rigid rotation shears the initial, purely poloidal bipolar magnetic field. This is different from the Sakurai wind presented above, where the boundary condition on B_φ was taken symmetric about the equator. Note how the equatorial acceleration to super-Alfvénic velocities occurs very close to the end of the dead zone. The critical surfaces are all displaced inwards as compared to the monopolar case.

Fig. 5 shows that poloidal streamlines and fieldlines are parallel. The E_φ is below 3%. In Fig. 6, we show the latitudinal variation of the (scaled) density and the velocity at two fixed radial distances in a polar plot. The spacecraft Ulysses and the on-board SWOOPS experiment provided the solar community with detailed measurements of these quantities for the solar wind (McComas et al. 1998). Qualitatively, the measured poloidal density and velocity variation resembles the curves from Fig. 6:

the density is higher about the ecliptic and there is a decrease in wind speed associated with the equatorial 'dead' zone. However, our computational domain extended to 50 stellar radii, while Ulysses measurements apply to larger radial distances. Note that we could use observed solar differential rotation profiles, as well as mass fluxes and magnetic field strengths, to obtain a better MHD proxy of solar wind conditions. The extent of the solar coronal active region belt suggests the use of a 'dead' zone larger than modeled in Fig. 5.

7. Conclusions and outlook

We obtained polytropic stellar winds as steady-state transonic outflows calculated with the Versatile Advection Code. We could relax an isothermal, spherically symmetric Parker wind, to a polytropic wind model. Subsequently, we included stellar rotation and a magnetic field, to arrive at the well-known Weber-Davis solution. We used fully implicit time stepping to converge to the steady-state solutions. The correctness of these 1D wind solutions can be checked *precisely*.

We generalized to 2D axisymmetric, unmagnetized and magnetized winds. Noteworthy is our prescription of the stellar boundary conditions in terms of the prescribed mass flux f_{mass} and the way in which the parallelism of the flow and the fieldlines in the poloidal plane is achieved. In Bogovalov (1996), the stellar boundary specified the normal magnetic field component and the density at the surface, while keeping the velocity of the plasma on the stellar surface in the rotating frame constant. Our approach differs markedly, since we impose the mass flux and ensure the correct rotational coupling of velocity and magnetic field. We refrain from fixing the density, as the analytical treatment shows that the algebraic Bernoulli equation together with the cross-field momentum balance really determines the density profile and the magnetic flux function concurrently, and should not be specified a priori. In fact, we let the density and all magnetic field components adjust freely at the base. This allows for the simultaneous and self-consistent modeling of both open and closed fieldline regions, which is not immediately possible when using the method of Sakurai (1985). By an appropriate initialization of the time-marching procedure used to get the steady-state solutions, we can find magnetized winds containing both a 'wind' and a 'dead' zone.

The method lends itself to investigate thermally and/or magneto-centrifugally driven polytropic wind solutions. One could derive angular momentum loss rates used in studies of stellar rotational evolution (Keppens et al. 1995, Keppens 1997). However, our immediate interest is in the relaxation of the assumptions inherent in our approach.

In this paper, we assume a polytropic equation of state throughout. All solutions are smooth and demonstrate a continuous acceleration from subslow outflow at the stellar surface to superfast outflow at large radial distances. Our polytropic assumption has to be relaxed to investigate the combined coronal heating/solar wind problem within an MHD context. This involves adding the energy equation. We plan to study possible discontinuous transonic solutions containing shocks. We

can then address the puzzling paradox recently raised by analytic investigations of translational symmetric and axisymmetric transonic MHD flows (Goedbloed & Lifschitz 1997, Lifschitz & Goedbloed 1997, Goedbloed et al. 1998). The generalized Grad-Shafranov equation describing the cross-fieldline force balance has to be solved concurrently with the algebraic condition expressed by the Bernoulli equation. Rigorous analysis of the generalized mixed-type Grad-Shafranov partial differential equation, in combination with the algebraic Bernoulli equation, shows that only shocked solutions can be realized whenever a limiting line appears within the domain of hyperbolicity. Moreover, in Goedbloed & Lifschitz (1997) and Lifschitz & Goedbloed (1997), it was pointed out that there are forbidden flow regimes for certain translationally symmetric, self-similar solutions of the MHD equations. The Alfvén critical point is in those solutions situated within a forbidden flow regime, which can only be crossed by shocks. It is of vital importance to understand what ramifications this has on analytic and numerical studies of stellar winds, or on accretion-type flows where shocked solutions are rule rather than exception. Since the schemes used in VAC are shock-capturing, we have all ingredients needed to clarify this paradox. Numerical studies of self-similar solutions as those discussed in Trussoni et al. (1996) and Tsinganos et al. (1996) are called for. Combined analytic and numerical studies of such axisymmetric steady-state flows have been initiated in Goedbloed et al. (1998) and in Ustyugova et al. (1998).

After those paradoxes are resolved, we will be in a position to relax the conditions of axisymmetry and stationarity. While several authors have already initiated this daunting task (Gibson & Low 1998, Guo & Wu 1998, Wu & Dryer 1997, Usmanov & Dryer 1995), we believe that an in-depth study of the subtleties involved with the various restrictions mentioned is still warranted.

References

Belcher J.W., MacGregor K.B., 1976, ApJ 210, 498

Bogovalov S.V., 1996, In: Tsinganos K. (ed.) Solar and astrophysical magnetohydrodynamic flows. Kluwer academic publishers, Dordrecht, 411

Bogovalov S.V., 1997, A&A 323, 634

Brackbill J.U., Barnes D.C., 1980, J. Comput. Phys. 35, 426

Charbonneau P., 1995, ApJS 101, 309

Collela P., Woodward P.R., 1984, J. Comput. Phys. 54, 174

Evans C.R., Hawley J.F., 1988, ApJ 332, 659

Gibson S.E., Low B.C., 1998, ApJ 493, 460

Goedbloed J.P., Lifschitz A., 1997, Phys. Plasmas 4 (10), 3544

Goedbloed J.P., Keppens R., Lifschitz A., 1998, In: Proceedings of 25th EPS conference on controlled fusion and plasma physics, June 29-July 3, Prague, Czech Republic

Guo W.P., Wu S.T., 1998, ApJ 494, 419

Holzer T.E., Leer E., 1997, In: Proceedings of the Fifth SOHO Workshop, The Corona and Solar Wind near Minimum Activity. ESA-SP-404, 65

Keppens R., 1997, A&A 318, 275

Keppens R., Tóth G., 1998, In: Proceedings of VECPAR'98 (3rd international meeting on vector and parallel processing), June 21–23, Porto, Portugal, Part II, 599

Keppens R., MacGregor K.B., Charbonneau P., 1995, A&A 294, 469

Keppens R., Tóth G., Botchev M.A., van der Ploeg A., 1998, Implicit and semi-implicit schemes in the Versatile Advection Code: algorithms, submitted for publication

Lifschitz A., Goedbloed J.P., 1997, J. Plasma Phys. 58, 61

McComas D.J., Bame S.J., Barraclough B.L., et al., 1998, Geophys. Res. Lett. 25 (1), 1

Parker E.N., 1958, ApJ 128, 664

Powell K.G., 1994, An approximate Riemann solver for magnetohydrodynamics (that works in more than one dimension), ICASE Report No 94-24, Langley, VA

Sakurai T., 1985, A&A 152, 121

Sakurai T., 1990, Computer Phys. Reports 12, 247

Tóth G., 1996, Astrophys. Lett. & Comm. 34, 245

Tóth G., 1997, In: Hertzberger B., Sloot P. (eds.) Proceedings of High Performance Computing and Networking Europe 1997. Lecture Notes in Computer Science 1225, Springer-Verlag, Berlin, 253

Tóth G., 1997, J. Comput. Phys. 138, 981

Tóth G., Keppens R., 1998, In: Sloot P., Bubak M., Hertzberger B. (eds.) High Performance Computing and Networking. Lecture Notes in Computer Science, Vol. 1401, Proceedings HPCN Europe 1998, Springer-Verlag, Berlin, 368

Tóth G., Odstrčil D., 1996, J. Comput. Phys. 128, 82

Tóth G., Keppens R., Botchev M.A., 1998, A& A 332, 1159

Trussoni E., Sauty C., Tsinganos K., 1996, In: Tsinganos K. (ed.) Solar and astrophysical magnetohydrodynamic flows. Kluwer academic publishers, Dordrecht, 383

Trussoni E., Tsinganos K., Sauty C., 1997, A&A 325, 1099

Tsinganos K., Sauty C., 1992, A&A 255, 405

Tsinganos K., Sauty C., Sulantzis G., Trussoni E., Contopoulos J., 1996, MNRAS 283, 811

Usmanov A.V., Dryer M., 1995, Sol. Phys. 159, 347

Ustyugova G.V., Koldoba A.V., Romanova M.M., Chechetkin V.M., Lovelace R.V.E., 1998, Magneto-Centrifugally Driven Winds: Comparison of MHD Simulations with Theory. ApJ, in press

van der Ploeg A., Keppens R., Tóth G., 1997, In: Hertzberger B., Sloot P. (eds.) Proceedings of High Performance Computing and Networking Europe 1997. Lecture Notes in Computer Science 1225, Springer-Verlag, Berlin, 421

van der Vorst H.A., 1992, SIAM J. Sci. Statist. Comput. 13, 631

Weber E.J., Davis L., 1967, ApJ 148, 217

Wu C., Dryer M, 1997, Sol. Phys. 173, 391

Yee H.C., 1989, A class of high-resolution explicit and implicit shock-capturing methods. NASA TM-101088